

Systematic Synthesis and Characterization of Single-Crystal Lanthanide Orthophosphate Nanowires

Yue-Ping Fang,[†] An-Wu Xu,^{*†} Rui-Qi Song,[†] Hua-Xin Zhang,[†] Li-Ping You,[§] Jimmy C. Yu,[‡] and Han-Qin Liu[†]

Contribution from the School of Chemistry and Chemical Engineering, Zhongshan University, Guangzhou, 510275, China; Department of Chemistry, The Chinese University of Hong Kong, Shatin, New Territories, Hong Kong, China; and Electron Microscopy Laboratory, Peking University, Beijing, 100084, China

Received July 15, 2003; E-mail: ccdc17@zsu.edu.cn

Abstract: A simple hydrothermal method has been developed for the systematic synthesis of lanthanide orthophosphate crystals with different crystalline phases and morphologies. It has been shown that pure LnPO_4 compounds change structure with decreasing Ln ionic radius: i.e., the orthophosphates from Ho to Lu as well as Y exist only in the tetragonal zircon (xenotime) structure, while the orthophosphates from La to Dy exist in the hexagonal structure under hydrothermal treatment. The obtained hexagonal structured lanthanide orthophosphate LnPO_4 (Ln = La, Ce, Pr, Nd, Sm, Eu, Gd, Tb, and Dy) products have a wirelike morphology. In contrast, tetragonal LnPO_4 (Ln = Ho, Er, Tm, Yb, Lu, Y) samples prepared under the same experimental conditions consist of nanoparticles. The obtained hexagonal LnPO_4 (Ln = La \rightarrow Tb) can convert to the monoclinic monazite structured products, and their morphologies remained the same after calcination at 900 °C in air (Hexagonal DyPO_4 is an exceptional case, it transformed to tetragonal DyPO_4 by calcination), while the tetragonal structure for (Ho \rightarrow Lu, Y) PO_4 remains unchanged by calcination. The resulting LnPO_4 (Ln = La \rightarrow Dy) products consist almost entirely of nanowires/nanorods with diameters of 5–120 nm and lengths ranging from several hundreds of nanometers to several micrometers. Europium doped LaPO_4 nanowires were also prepared, and their photoluminescent properties were reported. The optical absorption spectrum of CePO_4 nanowires was measured and showed some differences from that of bulk CePO_4 materials. The possible growth mechanism of lanthanide phosphate nanowires was explored in detail. X-ray diffraction, field-emission scanning electron microscopy, transmission electron microscopy, electron diffraction, infrared absorption spectra, X-ray photoelectron spectroscopy, optical absorption spectra, and photoluminescence spectra have been employed to characterize these materials.

Introduction

Dimensionality plays an important role in determining the properties of nanomaterials and in the synthesis of nanostructured materials with controlled morphology, size, chemical composition, and crystal structure.^{1–3} Due to the discovery of carbon nanotubes, a lot of one-dimensional (1D) nanomaterials have been extensively investigated during the past few decades because of their potential technological applications.^{4–7} Aside

from nanotubes,^{8–10} a variety of 1D nanowires including oxides,¹¹ metal and alloys,¹² semiconductors,¹⁴ metal chalcogenides,¹³ and polymers,¹⁵ and so forth have been synthesized

[†] Zhongshan University.

[‡] The Chinese University of Hong Kong.

[§] Peking University.

(1) Hu, J.; Odom, W.; Lieber, C. M. *Acc. Chem. Res.* **1999**, *32*, 435.

(2) Kovtyukhova, N. I.; Mallouk, T. E. *Chem.—Eur. J.* **2002**, *8*, 4355.

(3) Xia, Y.; Yang, P.; Sun, Y.; Wu, Y.; Mayers, B.; Gates, B.; Yin, Y.; Kim, F.; Yan, H. *Adv. Mater.* **2003**, *15*, 353 and references therein.

(4) Wu, Y.; Yan, H.; Huang, M.; Messer, B.; Song, J. H.; Yang, P. *Chem.—Eur. J.* **2002**, *8*, 1261.

(5) (a) Feldman, Y.; Wasserman, E.; Srolovita, D. J.; Tenne, R. *Science* **1995**, *267*, 222. (b) Brorson, M.; Hansen, T. W.; Jacobsen, C. J. H. *J. Am. Chem. Soc.* **2002**, *124*, 11582. (c) Rao, C. N. R.; Satishkumar, B. C.; Govindaraj, A.; Nath, M. *ChemPhysChem* **2001**, *2*, 78. (d) Tenne, R. *Chem.—Eur. J.* **2002**, *8*, 5297. (f) Remskar, M.; Mrzel, A.; Skraba, Z.; Jesih, A.; Ceh, M.; Demšar, J.; Stadelmann, P.; Lévy, F.; Mihailovic, D. *Science* **2001**, *292*, 479.

(6) Yan, H.; He, R.; Johnson, J.; Law, M.; Saykally, R.; Yang, P. *J. Am. Chem. Soc.* **2003**, *125*, 4728.

(7) Pan, Z. W.; Dai, Z. R.; Wang, Z. L. *Science* **2001**, *291*, 1947.

(8) Iijima, S. *Nature* **1991**, *354*, 56.

(9) (a) Xu, A. W.; Fang, Y. P.; You, L. P.; Liu, H. Q. *J. Am. Chem. Soc.* **2003**, *125*, 1494. (b) Yada, M.; Mihara, M.; Mouri, S.; Kuroki, M.; Kijima, T. *Adv. Mater.* **2002**, *14*, 309.

(10) Goldberger, J.; He, R.; Zhang, Y.; Lee, S.; Yan, H.; Choi, H. J.; Yang, P. *Nature* **2003**, *422*, 599.

(11) (a) Dai, Z. R.; Gole, J. L.; Stout, J. D.; Wang, Z. L. *J. Phys. Chem. B* **2002**, *106*, 1274. (b) Zhang, D.; Sun, L.; Yin, J.; Yan, C. *Adv. Mater.* **2003**, *15*, 1022. (c) Dai, Z. R.; Pan, Z. W.; Wang, Z. L. *J. Phys. Chem. B* **2002**, *106*, 902. (d) Wang, W.; Xu, C.; Wang, G.; Liu, Y.; Zheng, C. *Adv. Mater.* **2002**, *14*, 837. (e) Yang, P.; Lieber, C. M. *J. Mater. Res.* **1997**, *12*, 2981.

(12) (a) Zhang, Z.; Blom, D. A.; Gai, Z.; Thompson, J. R.; Shen, J.; Dai, S. *J. Am. Chem. Soc.* **2003**, *125*, 7528. (b) Sun, Y.; Gates, B.; Mayers, B.; Xia, Y. *Nano Lett.* **2002**, *2*, 165. (c) Murphy, C. J.; Jana, N. R. *Adv. Mater.* **2002**, *14*, 80.

(13) (a) Duan, X.; Lieber, C. M. *Adv. Mater.* **2000**, *12*, 298. (b) Duan, X.; Huang, Y.; Cui, Y.; Wang, J.; Lieber, C. M. *Nature* **2001**, *409*, 66. (c) Hanrath, T.; Korgel, B. A. *J. Am. Chem. Soc.* **2002**, *124*, 1424. (d) Ma, D. D.; Lee, C. S.; Au, F. C. K.; Tong, S. Y.; Lee, S. T. *Science* **2003**, *299*, 1874.

(14) (a) Geng, B.; Wang, G.; Jiang, A.; Xie, T.; Sun, S.; Meng, G.; Zhang, L. *Appl. Phys. Lett.* **2003**, *82*, 4791. (b) Yang, C.; Awschalom, D. D.; Stucky, G. D. *Chem. Mater.* **2002**, *14*, 1277. (c) Sone, E. D.; Zubarev, E. R.; Stupp, S. I. *Angew. Chem., Int. Ed.* **2002**, *41*, 1706.

(15) (a) Gao, M.; Huang, S.; Dai, L.; Wallace, G.; Gao, R.; Wang, Z. *Angew. Chem., Int. Ed.* **2000**, *39*, 3664. (b) Fu, M.; Zhu, Y.; Tan, R.; Shi, G. *Adv. Mater.* **2001**, *13*, 1874.

and their novel properties have also been extensively explored. These 1D nanostructured materials have been shown to play an important role as active components or interconnects in fabricating nanoscale electronic, optical, optoelectronic, electrochemical, and electromechanical devices.¹⁶ Notable examples of demonstrated applications include field-effect transistors (FETs),¹⁷ light-emitting diodes (LEDs),^{13b} single-electron transistors,¹⁸ biological and chemical sensors,¹⁹ photodetectors,²⁰ electron emitters,²¹ and ultraviolet lasers.⁶

Although a number of synthetic methodologies have been developed to fabricate and assemble 1D nanostructures,²² they often suffer from the requirements of high temperature, special conditions, tedious procedures, and catalysts or templates. Therefore, the development of practical methods for fabricating large numbers of 1D nanostructures at low cost is still a great challenge for future study. Chemical methods, on the other hand, seem to provide an alternative and intriguing strategy for generating 1D nanostructures with respect to material diversity, cost, versatility, synthetic tunability, and potential for large-volume production. Of the methods employed in the synthesis of 1D nanomaterials, hydrothermal methods have been regarded as effective routes to the fabrication of high-quality anisotropic nanomaterials.²³ Several solution-phase procedures have been demonstrated for generating 1D nanostructures.²⁴ More recently, some studies have been reported on the synthesis of lanthanide hydroxide nanotubes and nanowires/nanorods by hydrothermal processes.²⁵ Conventionally, bulk monazite-type (high-temperature phase) lanthanide phosphates have been prepared by solid-phase reaction at high temperature.²⁶ LnPO₄ and rare earth ion doped LnPO₄ nanoparticles or colloids have also been prepared by solution precipitation methods, and their photoluminescence properties have been studied.²⁷ However, previously there have been no systematic accounts of synthesis, characterization, and properties of LnPO₄ nanowires and the correlation between

LnPO₄ morphologies with the crystal structures. These details will be presented in this article, where we report a systematic synthesis and characterization of high-quality LnPO₄ and lanthanide ion doped LnPO₄ single-crystal nanowires with controlled crystal phases obtained by hydrothermal treatment. The measurements of the photoluminescence emission and photoluminescence excitation spectra of rare earth activated LnPO₄ nanowires/nanorods were performed. The growth mechanism of LnPO₄ nanowires is also discussed based on the inherent crystal structure of these materials.

Orthophosphates are substances that are composed of isolated PO₄ tetrahedra, analogous to “orthosilicates”. The most common naturally occurring orthophosphates are apatite [Ca₅(PO₄)₃(F, Cl, OH)] and monazite (LnPO₄), where Ln refers to lanthanide elements. Lanthanide phosphates have several polymorphic forms. They appear in hexagonal, tetragonal, and monoclinic modifications. The hexagonal structure is the low-temperature phase, and it can transform into the monoclinic structure, while the tetragonal maintains its structure after calcination at 900 °C.^{28–31} Lanthanide compounds have been extensively used as high performance luminescent devices, magnets, catalysts, time-resolved fluorescence labels for biological detection, and other functional materials based on the electronic, optical, and chemical characteristics resulting from the 4f shell of their ions.³² Lanthanide orthophosphates (LnPO₄) have a variety of potentially beneficial properties, including very low solubility in water (their solubility products are on the level of 10⁻²⁵ to 10⁻²⁷),³³ high thermal stability (the melting points of LnPO₄ are around 2300 °C),³⁴ high index of refraction, and, in the cases of Nd, Eu, etc., high concentrations of lasing ions.³⁵ These properties provide the basis for interest in their use in a wide range of applications such as phosphors, sensors, proton conductors, ceramic materials, catalysts, and heat-resistant materials.^{36,37} Very recently, lanthanide phosphates have been of interest for use as inert matrixes for Pu fuel and as multilayered (with Al₂O₃ and ZrO₂) weak-bonded ceramic composites.³⁸ They also have

- (16) (a) Huang, Y.; Duan, X.; Wei, Q.; Lieber, C. M. *Science* **2001**, *291*, 630. (b) Huang, M. H.; Mao, S.; Feick, H.; Yan, H.; Wu, Y.; Kind, H.; Weber, E.; Russo, R.; Yang, P. *Science* **2001**, *292*, 1897. (c) Wang, Z. L. *Adv. Mater.* **2000**, *12*, 1295. (d) Dekker, C. *Phys. Today* **1999**, May 22. (e) Frank, S.; Poncharal, P.; Wang, Z. L.; de Heer, W. A. *Science* **1998**, *280*, 1744.
- (17) (a) Chung, S. W.; Yu, J. Y.; Heath, J. R. *Appl. Phys. Lett.* **2000**, *76*, 2068. (b) Tans, J. S.; Verschueren, R. M.; Dekker, C. *Nature* **1998**, *393*, 49.
- (18) (a) Tans, S. J.; Devoret, M. H.; Dal, H.; Thess, A.; Smalley, R. E.; Gerlligs, L. J.; Dekker, C. *Nature* **1997**, *386*, 474. (b) Bockrath, M.; Cobden, D. H.; MeEuen, P. L.; Chopra, N. G.; Zettl, A.; Thess, A.; Smalley, R. E.; *Science* **1997**, *275*, 1922.
- (19) (a) Cui, Y.; Wei, Q.; Park, H.; Lieber, C. M. *Science* **2001**, *293*, 1289. (b) Nicewarner-Peña, S. R.; Freeman, R. G.; Reiss, B. D.; He, L.; Peña, D. J.; Walton, I. D.; Cromer, R.; Keating C. D.; Natan, M. J. *Science* **2001**, *294*, 137.
- (20) Wang, J.; Gudiksen, M. S.; Duan, X.; Cui, Y.; Lieber, C. M. *Science* **2001**, *293*, 1455.
- (21) Davydov, D. N.; Sattari, P. A.; AlMawlawi, D.; Osika, A.; Haslett, T. L.; Moskovits, M. *J. Appl. Phys.* **1999**, *86*, 3983.
- (22) (a) Wu, Y.; Yan, H.; Huang, M.; Messer, B.; Song, J. H.; Yang, P. *Chem.—Eur. J.* **2002**, *8*, 1261. (b) Zhu, H.; Xu, C.; Wu, D.; Wei, B.; Vajtai, R.; Ajayan, P. M. *Science* **2002**, *296*, 884. (c) Brorson, M.; Hansen, T. W.; Jacobsen, C. J. *J. Am. Chem. Soc.* **2002**, *124*, 11582. (d) Ajayan, P. M.; Stephan, O.; Redlich, P.; Colliex, C. *Nature* **1995**, *375*, 564. (e) Han, W.; Fan, S.; Li, Q.; Hu, Y. *Science* **1997**, *277*, 1287. (f) Routkevitch, D.; Bigioni, T.; Moskovits, M.; Xu, J. M. *J. Phys. Chem.* **1996**, *100*, 14037.
- (23) Patzke, G. R.; Krumeich, F.; Nesper, R. *Angew. Chem., Int. Ed.* **2002**, *41*, 2446.
- (24) (a) Niederberger, M.; Muhr, H.-J.; Krumeich, F.; Bieri, F.; Günther, D.; Nesper, R. *Chem. Mater.* **2000**, *12*, 1995. (b) Kuang, D. B.; Xu, A. W.; Fang, Y. P.; Ou, H. D.; Liu, H. Q. *J. Cryst. Growth* **2002**, *244*, 379. (c) Vayssieres, L. *Adv. Mater.* **2003**, *15*, 464. (d) Holmes, J. D.; Johnston, K. P.; Doty, R. C.; Korgel, B. A. *Science*, **2000**, *287*, 1471.
- (25) (a) Xu, A. W.; Fang, Y. P.; You, L. P.; Liu, H. Q. *J. Am. Chem. Soc.* **2003**, *125*, 1494. (b) Wang, X.; Li, Y. D. *Angew. Chem., Int. Ed.* **2002**, *41*, 4790.
- (26) (a) Kizilyalli, M.; Welch, A. J. E. *J. Appl. Crystallogr.* **1976**, *9*, 413. (b) Mullica, D. F.; Milligan, W. O.; Grossie, D. A. Beall, G. W.; Boatner, L. A. *Inorg. Chim. Acta* **1984**, *95*, 231. (c) Wang, R.; Pan, W.; Chen, J.; Fang, M.; Cao, Z.; Luo, Y. *Mater. Chem. Phys.* **2003**, *79*, 30.
- (27) (a) Riwotzki, K.; Meyssamy, H.; Schnablegger, H.; Kornowski, A.; Haase, M. *Angew. Chem., Int. Ed.* **2001**, *40*, 573. (b) Haase, M.; Riwotzki, K.; Meyssamy, H.; Kornowski, A. *J. Alloys Compd.* **2000**, *303–304*, 191. (c) Heer, S.; Lehmann, O.; Haase, M.; Güdel, H. U. *Angew. Chem., Int. Ed.* **2003**, *42*, 3179. (d) Riwotzki, K.; Meyssamy, H.; Kornowski, A.; Haase, M. *J. Phys. Chem. B* **2000**, *104*, 2824. (e) Kijkowska, R. *J. Mater. Sci.* **2003**, *38*, 229.
- (28) Hezel, A.; Ross, S. D. *J. Inorg. Nucl. Chem.* **1967**, *29*, 2085.
- (29) Meldrum, A.; Boatner, L. A.; Ewing, R. C. *Phys. Rev. B* **1997**, *56*, 13805.
- (30) Kijkowska, R.; Cholewka, E.; Duszak, B. *J. Mater. Sci.* **2003**, *38*, 223.
- (31) (a) Li, B.; Shen, L.; Liu, X.; Wang, T.; Ishii, K.; Sakaki, Y.; Kashiwaya, Y.; Takahashi, H.; Shibayama, T. *J. Mater. Sci. Lett.* **2000**, *19*, 343. (b) Onoda, H.; Nariai, H.; Maki, H.; Motooka, I. *Mater. Chem. Phys.* **2002**, *73*, 19.
- (32) (a) Adachi, G. Y.; Imanaka, N. *Chem. Rev.* **1998**, *98*, 1479. (b) Xu, A. W.; Gao, Y.; Liu, H. Q. *J. Catal.* **2002**, *207*, 151. (c) Peruski, A. H.; Johnson, L. H.; Peruski, L. F. *J. Immunol. Methods* **2002**, *263*, 35–41. (d) Capobianco, J. A.; Boyer, J. C.; Vetrone, F.; Speghini, A.; Bettinelli, M. *Chem. Mater.* **2002**, *14*, 2915. (e) Dhanaraj, J.; Jagannathan, R.; Kutty, T. R. N.; Lu, C. H. *J. Phys. Chem. B* **2001**, *105*, 11098.
- (33) Firsching, F. H.; Brune, S. N. *J. Chem. Eng. Data* **1991**, *36*, 93.
- (34) Rouanel, E.; Serra, J. J.; Allaf, K.; Orlovskii, V. P. *Inorg. Mater.* **1981**, *17*, 76.
- (35) Guo, Y.; Woznicki, P.; Barkatt, A.; Saad, E. E.; Talmy, I. G. *J. Mater. Res.* **1996**, *11*, 639.
- (36) (a) Nishihama, S.; Hirai, T.; Komasa, I. *J. Mater. Chem.* **2002**, *12*, 1053. (b) Onoda, H.; Nariai, H.; Moriwaki, A.; Maki, H.; Motooka, I. *J. Mater. Chem.* **2002**, *12*, 1754.
- (37) Ordonez-Regil, E.; Drot, R.; Simoni, E.; Ehrhardt, J. J. *Langmuir* **2002**, *18*, 7977.
- (38) (a) Uskakov, S. V.; Helean, K. B.; Navrotsky, A.; Boatner, L. A. *J. Mater. Res.* **2001**, *16*, 2623. (b) Matzke, H.; Rondinella, V. V.; Wiss, T. *J. Nucl. Mater.* **1999**, *274*, 47. (c) Kleykamp, H. *J. Nucl. Mater.* **1999**, *275*, 1. (d) Marshall, D. B.; Morgan, P. E.; Housley, R. M. *J. Am. Ceram. Soc.* **1997**, *80*, 1677. (e) Mawdsley, J. R.; Kovar, D.; Halloran, J. W. *J. Am. Ceram. Soc.* **2000**, *83*, 802.

properties that make them of interest as scintillators for X-ray and γ -ray detection in medical imaging applications, as thermophosphors for remote temperature measurements, and as hosts for microlasers.³⁹ Recently, ceramic LaPO_4 doped with 1–5 mol % Sr has been found to exhibit proton conduction in a wet atmosphere at high temperature. Such solid-state protonic conductors are candidates as electrolytes in fuel cells, hydrogen separation membranes, and sensors.⁴⁰ Lanthanide phosphates have been shown to be a useful host lattice for lanthanide ions to produce phosphors emitting a variety of colors.^{27,41} Ce^{3+} and Tb^{3+} coactivated bulk LaPO_4 is a highly efficient and commercially applied green (${}^3\text{D}_4\text{--}{}^7\text{F}_5$ of Tb^{3+} at 543 nm) phosphor in fluorescent lamps.^{27a,42} In compact lamps, the wall temperature is in the range of 150–200 °C. At these temperatures, most lamp phosphors degrade, but $\text{LaPO}_4/\text{Ce}/\text{Tb}$ phosphor is stable at high temperatures.⁴² Nanoscaled phosphors could have some potential advantages over conventional micron-sized phosphors.⁴³ The properties of lanthanide compounds depend strongly on the compositions and structure, which are sensitive to the bonding states of lanthanide ions. If lanthanide compounds were fabricated in the form of a 1D nanostructure (e.g., nanowires) with a different crystal structure, they would have new functionalities as a result of their marked specific shape. They would also act as electrically, magnetically, or optically functional host materials for rare earth ions in phosphor displays, waveguide devices, fluorescence labels for biological detection, and the active material in lasers.⁴⁴

Experimental Section

Preparation. Hexagonal ($\text{La} \rightarrow \text{Dy}$) PO_4 nanowires (or nanorods) and tetragonal ($\text{Ho} \rightarrow \text{Lu}$, Y) PO_4 nanoparticles were prepared by a simple hydrothermal method. In a typical synthesis, 10 mL of $\text{NH}_4\text{H}_2\text{PO}_4$ (0.4 M) aqueous solution were added into 10 mL of $\text{Ln}(\text{NO}_3)_3$ ($\text{Ln} = \text{La}, \text{Ce}, \text{Pr}, \text{Nd}, \text{Sm}, \text{Eu}, \text{Gd}, \text{Tb}, \text{Dy}, \text{Ho}, \text{Er}, \text{Tm}, \text{Yb}, \text{Lu}$, and nonlanthanide Y) aqueous solution (0.4 M) under vigorous stirring for 20 min. The pH was adjusted to a specific value using aqueous ammonia (27 wt %) solution. The resulting suspension was poured into a Teflon-lined stainless steel autoclave. The autoclave was sealed and maintained at 150 °C for 12 h and then air cooled to room temperature. The resulting LnPO_4 products were filtered, washed with deionized water and absolute alcohol to remove ions possibly remaining in the final products, and finally dried at 80 °C in air for further characterization. LaPO_4 nanowires doped with 5 mol % europium were prepared according to the same method. To prepare CePO_4 nanowires, the suspension in the autoclave was first purged with argon for 60 min to prevent oxidation of Ce^{3+} to Ce^{4+} before heating. Monoclinic ($\text{La} \rightarrow \text{Tb}$) PO_4 and tetragonal DyPO_4 nanowires/nanorods were prepared by calcination of hydrothermally obtained corresponding products at 900 °C in air.

Characterization. The X-ray powder diffraction (XRD) patterns of all samples were performed on a Rigaku/Max-3A X-ray diffractometer with $\text{Cu K}\alpha$ radiation ($\lambda = 1.5418 \text{ \AA}$). The operation voltage and current were maintained at 40 kV and 40 mA, respectively. Field-emission scanning electron microscopic (FE-SEM) images were obtained with a JEOL JSM-6330F operated at a beam energy of 10.0 kV. Transmission electron microscopic (TEM) images, high-resolution transmission electron microscopic (HRTEM) images, and the selected area electron diffraction (SAED) patterns were obtained on a JEOL-2010 microscope with an accelerating voltage of 200 kV. Energy-dispersive X-ray spectroscopy (EDS) was attached to the JEOL 2010. Sample grids were prepared by sonicating powdered samples in ethanol for 20 min and evaporating one drop of the suspension onto a carbon-coated, holey film supported on a copper grid for TEM measurements. A Shimadzu spectrophotometer (model 2501 PC) equipped with an integrating sphere was used to record the UV–vis diffuse reflectance spectra of the samples. The excitation and emission spectra were recorded with an F-4500 spectrophotometer equipped with a 150 W xenon lamp as the excitation source. All the measurements were performed at room temperature. Fourier transform infrared spectroscopy (FTIR) analysis was carried out using KBr disks in the region of 4000–400 cm^{-1} by using FTIR-Bruker-EQUINOX-55 at ambient conditions. X-ray photoelectron spectroscopy (XPS) measurements were performed in a VG Scientific ESCALAB Mark II spectrometer equipped with two ultra-high-vacuum (UHV) chambers. All binding energies were referenced to the $\text{C}1\text{s}$ peak at 284.8 eV of the surface adventitious carbon.

Results and Discussion

I. Synthesis and Characterization of Hexagonal ($\text{La} \rightarrow \text{Dy}$)- PO_4 Nanowires and Tetragonal ($\text{Ho} \rightarrow \text{Lu}$, Y) PO_4 Crystals.

Under identical synthetic conditions (at 150 °C for 12 h, pH 1–2), two different types of crystal structure of the obtained LnPO_4 products have been identified by X-ray diffraction (XRD) analyses. XRD patterns of the obtained hexagonal LnPO_4 ($\text{Ln} = \text{La}, \text{Ce}, \text{Pr}, \text{Nd}, \text{Sm}, \text{Eu}, \text{Gd}, \text{Tb}, \text{Dy}$) nanowires/nanorods and tetragonal ($\text{Ho} \rightarrow \text{Lu}$, Y) PO_4 nanoparticles are shown in Figures S1 and S2 (Supporting Information), respectively. All the peaks of the XRD patterns for each sample in Figure S1 can be readily indexed to a pure hexagonal phase [space group: $P3_121$ (152)] of ($\text{La} \rightarrow \text{Dy}$) PO_4 , in good agreement with the data in the JCPDS cards. XRD results show that all nine LnPO_4 ($\text{Ln} = \text{La} \rightarrow \text{Dy}$) crystals are isostructural. Moreover, the intensity of the (200) peak is much stronger than those of the other peaks, which is different from bulk hexagonal LnPO_4 ($\text{Ln} = \text{La} \rightarrow \text{Dy}$).³⁰ This indicates that the obtained LnPO_4 ($\text{Ln} = \text{La} \rightarrow \text{Dy}$) nanowires/nanorods grow preferentially along the [001] direction (the c axis). This is further demonstrated below by HRTEM and ED measurements. All diffraction peaks shown in Figure S2 are characteristic of a pure tetragonal phase [space group: $I4_1/amd$ (141)] of ($\text{Ho} \rightarrow \text{Lu}$, Y) PO_4 (the nonlanthanide YPO_4 also has a tetragonal structure, so it is included in the present study). It can be seen that six ($\text{Ho} \rightarrow \text{Lu}$, Y) PO_4 samples are isostructural. Moreover, XRD analyses show systematic shifts in the positions of the diffraction peaks reflecting the contraction of the ionic radii of the lanthanides, as clearly seen from Figures S1 and S2. The unit cell dimensions of all LnPO_4 crystals calculated from XRD patterns are consistent with those reported in the JCPDS cards.

The measured lattice parameters a and c , plotted against the revised crystal (CR) ionic radii of the eight-coordinated three-valent lanthanide cations,⁴⁵ are presented in Figure 1. The

- (39) (a) Moses, W. W.; Weber, M. J.; Derezno, S. E.; Perry, D.; Berdahl, P.; Boatner, L. A. *IEEE Trans. Nucl. Sci.* **1998**, *45*, 462. (b) Allison, S. W.; Boatner, L. A.; Gillies, G. T. *Appl. Opt.* **1995**, *25*, 5624. (c) Rapaport, A.; David, V.; Bass, M.; Deka, C.; Boatner, L. A. *J. Lumin.* **1999**, *85*, 155. (40) (a) Norby, T.; Christiansen, N. *Solid State Ionics* **1995**, *77*, 240. (b) Amezawa, K.; Maekawa, H.; Tomii, Y.; Yamamoto, N. *Solid State Ionics* **2001**, *145*, 233. (c) Tyholdt, F.; Horst, J. A.; Jørgensen, S.; Østvold, T.; Norby, T. *Surf. Interface Anal.* **2000**, *30*, 95. (41) (a) Dexpert-Ghys, J.; Mauricot, R.; Faucher, M. D. *J. Lumin.* **1996**, *69*, 203. (b) Rambabu, U.; Munirathnam, N. R.; Prakash, T. L.; Buddhudu, S. *Mater. Chem. Phys.* **2002**, *78*, 160. (c) Wu, X.; You, H.; Cui, H.; Zeng, X.; Hong, G.; Kim, C. H.; Pyun, C. H.; Yu, B. Y.; Park, C. H. *Mater. Res. Bull.* **2002**, *37*, 1531. (42) (a) Kang, Y.; Kim, E. J.; Lee, D. Y.; Park, H. D. *J. Alloys Compd.* **2002**, *347*, 266. (b) Lenggoro, I. W.; Xia, B.; Mizushima, H.; Okuyama, K.; Kijima, N. *Mater. Lett.* **2001**, *50*, 92. (43) (a) Bhargava, R. N.; Gallagher, D.; Hong, X.; Nurmikko, A. *Phys. Rev. Lett.* **1994**, *72*, 416. (b) Holmes, J. D.; Ziegler, K. J.; Doty, R. C.; Pell, L. E.; Johnston, K. P.; Korgel, B. A. *J. Am. Chem. Soc.* **2001**, *123*, 3743. (44) (a) Schuetz, P.; Caruso, F. *Chem. Mater.* **2002**, *14*, 4509. (b)

- (45) Shannon, R. D. *Acta Crystallogr. A* **1976**, *32*, 751.

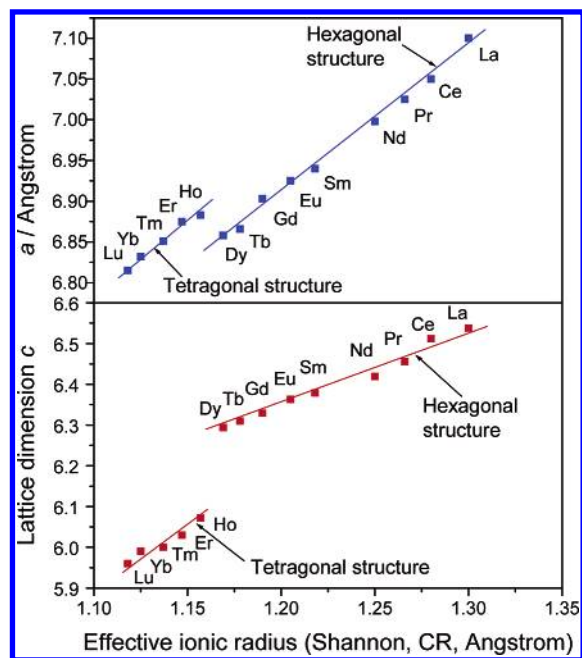


Figure 1. Plots of the measured lattice constants a (top) and c (bottom) of the obtained hexagonal and tetragonal LnPO_4 against lanthanide ionic radius.

approximately linear plots show the expected effect of the lanthanide contraction. On the other hand, it is clearly observed from Figure 1 that La, Ce, Pr, Nd, Sm, Eu, Gd, Tb, and Dy are located at one line and that their phosphates have a hexagonal structure, while Ho, Er, Tm, Yb, and Lu are located on the other line and their phosphates have a tetragonal structure. Why does LnPO_4 ($\text{Ln} = \text{La} \rightarrow \text{Dy}$) have a hexagonal structure and ($\text{Ho} \rightarrow \text{Lu}, \text{Y}$) PO_4 crystallize in a tetragonal structure under the same synthetic conditions? It is believed that this could be associated with the change of lanthanide ion radius, although the exact reason is not clear at present. In fact, the same phenomena have also been observed for LnPO_4 crystals prepared directly by solid-phase reaction at high temperature (900–1300 °C). It is found that LnPO_4 ($\text{Ln} = \text{La} \rightarrow \text{Dy}$) crystallize in the monoclinic form, while ($\text{Ho} \rightarrow \text{Lu}, \text{Y}$) PO_4 exist in the tetragonal structure under direct solid-phase reaction conditions. Obviously, the monoclinic is a high-temperature phase, and the hexagonal is a low-temperature phase; the structure transition from the hexagonal to the monoclinic can be observed by calcination at high temperature. This will be further demonstrated below.

The morphology of the samples was examined with scanning electron microscopy (SEM) and transmission electron microscopy (TEM). SEM images of the obtained PrPO_4 , SmPO_4 , GdPO_4 , TbPO_4 , and DyPO_4 nanowires/nanorods are shown in Figures 2a, b, c, d, and S3e, respectively, and shown in Figure 3a, b, S3c, and S3d (Figure S3, Supporting Information) are the TEM images of the obtained LaPO_4 , CePO_4 , NdPO_4 , and EuPO_4 nanowires/nanorods, respectively. The as-synthesized LnPO_4 ($\text{Ln} = \text{La} \rightarrow \text{Dy}$) products consist almost entirely of nanowires/nanorods with diameters of 5–120 nm and lengths ranging from several hundreds of nanometers to several micrometers. The high density of nanowires is representative of the high yields (close to 100%) associated with this new preparation approach. The results demonstrate that high-quality hexagonal structured LnPO_4 ($\text{Ln} = \text{La} \rightarrow \text{Dy}$) nanowires/nanorods can be obtained by this simple method. It is worth

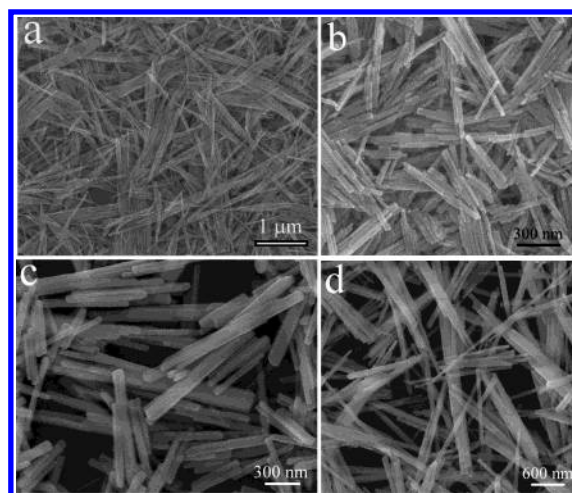


Figure 2. SEM images of the as-synthesized LnPO_4 nanowires by hydrothermal treatment. (a) PrPO_4 , (b) SmPO_4 , (c) GdPO_4 , (d) TbPO_4 .

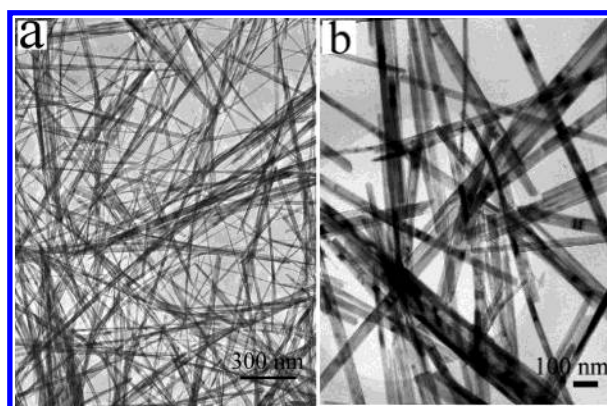


Figure 3. TEM images of the obtained hexagonal LaPO_4 (a) and CePO_4 (b) nanowires or nanorods.

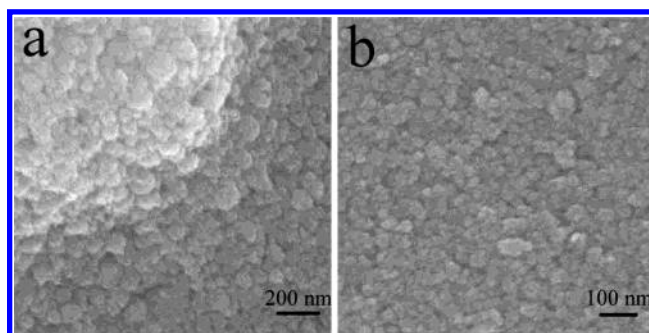


Figure 4. SEM images of the obtained tetragonal ErPO_4 (a) and LuPO_4 (b) nanoparticles.

noting that DyPO_4 nanowires aggregate into large bundles, as clearly shown in Figure S3e (Figure S3, Supporting Information).

Under the same synthetic conditions, ($\text{Ho} \rightarrow \text{Lu}, \text{Y}$) PO_4 crystals with particle morphology can be observed. Figure 4a and b shows SEM images of the obtained tetragonal structured ErPO_4 and LuPO_4 crystals, respectively. YPO_4 , HoPO_4 , TmPO_4 , and YbPO_4 can also be obtained only in the form of irregularly shaped particles. No rodlike morphology can be observed for ($\text{Ho} \rightarrow \text{Lu}, \text{Y}$) PO_4 samples.

The morphology and structure of the products were further characterized by TEM and HRTEM. TEM and HRTEM images and the selected area electron diffraction (SAED) patterns of

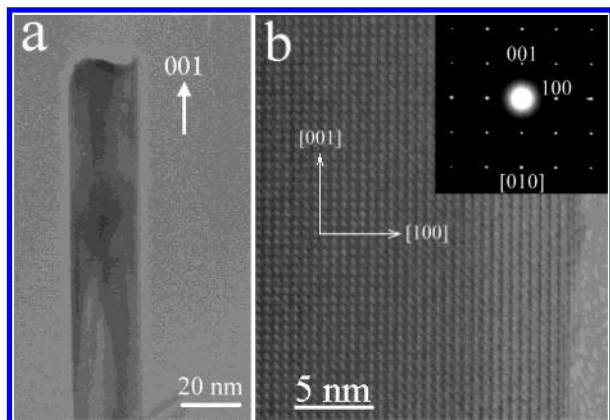


Figure 5. (a) TEM image of a single CePO_4 nanowire. (b) HRTEM image of a single nanowire with the clear lattice fringes of [001] with a spacing 0.652 nm and [100] with a spacing 0.608 nm. Inset in part b: the corresponding electron diffraction shows a single crystal recorded from the [010] zone axis.

CePO_4 , GdPO_4 , and DyPO_4 are presented in Figures 5, S4, and S5 (Figures S4 and S5, Supporting Information), respectively. Figures 5a, S4a, and S5a show the low magnification TEM images of the obtained LnPO_4 nanowires, further demonstrating that the obtained products have wirelike morphology. The HRTEM images (Figures 5b, S4b, and S5c) taken from a single nanowire show the clearly resolved planes of (001) and (100). The (001) planes are oriented parallel to the nanowire growth axis, indicating that the direction of nanowire growth is along the c axis. The SAED pattern (inset in Figures 5b, S4b, S5b) taken from a single nanowire can be indexed as a hexagonal LnPO_4 single crystal recorded from the [010] zone axis. The same results were also obtained for the six other LnPO_4 nanowires/nanorods. TEM observations for all wirelike samples show that each nanowire has a single crystal and that the growth direction of nine LnPO_4 nanowires/nanorods is the same, along the c axis, in good agreement with the XRD analyses. Energy-dispersive X-ray spectroscopy (EDS) analysis shows that the sample contains Ln, P, and O elements (Figure S6, Supporting Information). The composition of the products as extracted from the EDS analysis gives an Ln/P/O atomic ratio of $\sim 1:1:4.2$, in agreement with LnPO_4 .

Figure S7 (Supporting Information) shows FTIR spectra of the obtained LnPO_4 ($\text{Ln} = \text{La} \rightarrow \text{Dy}$) and $(\text{Ho} \rightarrow \text{Lu}, \text{Y})\text{PO}_4$ samples. Present FTIR data for lanthanide orthophosphates agree with reported values⁴⁶ and show the presence of a discrete PO_4 group; no pyrophosphate (P_2O_7 group, a typical band appearing at $1265\text{--}1267\text{ cm}^{-1}$) impurity could be detected. There is a noticeable shift in the absorption frequencies depending on different lanthanide phosphates. For example, the absorption peak (615 or 951 cm^{-1} for LaPO_4) is systematically shifting into a higher frequency (626 or 985 cm^{-1} for DyPO_4) from LaPO_4 to DyPO_4 , as clearly indicated in Figure S7. The systematic frequency shifts can be associated with the decrease in ionic radius from La^{3+} to Dy^{3+} (the effect of the lanthanide contraction).

The products obtained were further examined by XPS analysis. The XPS spectra of hexagonal LaPO_4 nanowires shown in Figure S8 (Supporting Information) give further evidence for the composition and purity of the products. All the peaks were

calibrated by using C 1s (284.8 eV) as the reference. The binding energies of the XPS peaks are consistent with that reported for bulk LaPO_4 .^{40c,47} The peak at 133.8 eV (P 2p) suggests that phosphorus in the products exists as pentavalent oxidation states (P^{5+}).⁴⁸ The atomic ratio of La to P based on semiquantitative XPS analysis is about 1:1. The XPS data demonstrate that the product is pure LaPO_4 , which agrees with the results of XRD and FTIR analyses. The XPS results for other lanthanide phosphates also illustrate that the products were completely formed in the stoichiometric ratio and that P exists in the P^{5+} state (data not shown here).

Controlled experiments were carried out to investigate the influence of pH and hydrothermal reaction temperature on the synthesis of LnPO_4 samples and the phase evolution. It is found that pH has some effect on the length and aspect ratio of the nanowires but little on the morphology of the nanowires. LnPO_4 ($\text{La} \rightarrow \text{Dy}$) nanowires were always obtained at pH 1–7. Hexagonal LnPO_4 ($\text{Ce} \rightarrow \text{Dy}$) nanowires were obtained at pH 1–7 by a hydrothermal process at $150\text{ }^\circ\text{C}$ for 12 h. Increasing the pH of the precursor mixture resulted in an increase in the lengths and aspect ratios of the nanorods. As for LaPO_4 , when the pH of the precursor suspension was increased to 4–5, the product after a hydrothermal treatment at $150\text{ }^\circ\text{C}$ for 12 h had a monoclinic structure and wirelike morphology (data not shown). The reaction temperature can cause the phase evolution. When temperature was increased to $220\text{ }^\circ\text{C}$, monoclinic LnPO_4 ($\text{La} \rightarrow \text{Tb}$) nanorods/nanowires were obtained at pH 1–7, and the obtained $(\text{Ho} \rightarrow \text{Lu}, \text{Y})\text{PO}_4$ nanoparticles have a tetragonal structure. Below pH 1, no precipitate was obtained. When the pH was increased over 7, the mixture of LnPO_4 and lanthanide hydroxides was obtained. Our results demonstrate that LnPO_4 ($\text{La} \rightarrow \text{Dy}$) nanowires prepared at $150\text{ }^\circ\text{C}$ for 12 h, pH 1–2 all have a hexagonal structure.

II. Structure Transition of LnPO_4 from Hexagonal to Monoclinic after Calcination. After all LnPO_4 samples obtained by hydrothermal treatment were calcined at $900\text{ }^\circ\text{C}$ in air for 3 h, it was found that the hexagonal structure for LnPO_4 ($\text{La} \rightarrow \text{Tb}$) nanowires/nanorods transforms into the monoclinic structure for corresponding materials. The hexagonal DyPO_4 is an exceptional case, and it converts to the tetragonal structure. Tetragonal $(\text{Ho} \rightarrow \text{Lu}, \text{Y})\text{PO}_4$ samples maintain their original structure after calcination. Moreover, the morphology of nanowires was not altered by calcination. Figure S9 (Supporting Information) shows XRD patterns of the obtained monoclinic LnPO_4 products by calcination, and from the figure it is clear that all the diffraction peaks for each sample could be indexed to a pure monoclinic phase [space group: $P2_1/n$ (14)] of $(\text{La} \rightarrow \text{Tb})\text{PO}_4$, in agreement with the reported data in the JCPDS cards. As for the hexagonal DyPO_4 sample, the tetragonal structure was obtained after calcination (Figure S10, bottom, Supporting Information). The XRD patterns of the calcined YPO_4 and HoPO_4 products are shown in Figure S10, and from the figure it is clearly seen that the tetragonal structure in the $(\text{Ho} \rightarrow \text{Lu}, \text{Y})\text{PO}_4$ samples remains unchanged (the calcined ErPO_4 , TmPO_4 , YbPO_4 , and LuPO_4 samples all have the tetragonal structure; data not shown here). TEM images of the

(47) Jørgensen, S.; Horst, J. A.; Dyrli, O.; Larring, Y.; Ræder, H.; Norby, T. *Surf. Interface Anal.* **2002**, *34*, 306 (XPS).

(48) (a) Splinter, S. J.; Rofagha, R.; McIntyre, N. S.; Erb, U. *Surf. Interface Anal.* **1996**, *26*, 471. (b) Yu, J. C.; Zhang, L. Z.; Zheng, Z.; Zhao, J. C. *Chem. Mater.* **2003**, *15*, 2280.

(46) Hezel, A.; Ross, S. D. *Spectrochim. Acta* **1966**, *22*, 1949.

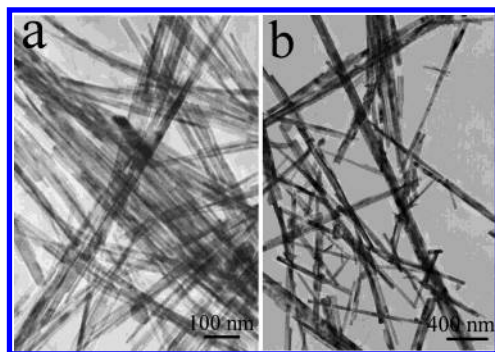


Figure 6. TEM images of monoclinic LnPO_4 nanowires/nanorods obtained by calcination of as-made corresponding products at $900\text{ }^\circ\text{C}$. (a) LaPO_4 , (b) CePO_4 .

obtained monoclinic LaPO_4 , CePO_4 , PrPO_4 , and tetragonal DyPO_4 nanowires/nanorods are presented in Figures 6a, 6b, S11c, and S11d (Figure S11, Supporting Information), respectively. It is clearly shown that the morphologies of nanowires/nanorods have remained the same after calcination at high temperature, indicating that LnPO_4 nanowires/nanorods are very stable. With close examinations of each nanowire/nanorod by TEM, we found that the surfaces of nanowires/nanorods become coarser as compared to those of corresponding hexagonal materials, an effect which is believed to be caused by calcination.

It is worth noting that DyPO_4 is an exceptional case. According to previous studies,³⁰ it can crystallize in the hexagonal, monoclinic, or tetragonal form. In fact, all $(\text{La} \rightarrow \text{Dy})\text{PO}_4$ can only crystallize in a monoclinic structure when directly prepared by a solid-phase reaction at high temperature,^{26a} while $(\text{Ho} \rightarrow \text{Lu}, \text{Y})\text{PO}_4$ have the tetragonal structure when prepared by the same method.⁴⁹ As compared with LnPO_4 prepared by a hydrothermal method, the same phenomena for crystal phase change can also be observed for LnPO_4 obtained directly by high-temperature solid-phase synthesis. We have also prepared DyPO_4 crystals by a direct solid-phase reaction and found that only a monoclinic structure can be observed for DyPO_4 . Why does the hexagonal structure for DyPO_4 nanowires obtained by the hydrothermal method convert to the tetragonal but not the monoclinic after calcination? Figure 1 shows that DyPO_4 exists in the boundary positions between the hexagonal and the tetragonal, which also indicates that DyPO_4 may crystallize in the tetragonal phase under certain conditions. Overall, DyPO_4 crystals can be obtained either in the tetragonal phase or in the monoclinic phase depending on the experimental conditions.

III. Absorption Spectra of CePO_4 Nanowires. Cerium compounds such as CePO_4 , CeP_2O_7 , and CeO_2 have been known to have strong absorption for the ultraviolet.⁵⁰ The optical absorption spectra of CePO_4 nanowires were measured and compared with those of bulk CePO_4 . The absorption spectra of CePO_4 nanowires (red line) and bulk CePO_4 (blue line) are shown in Figure 7. The observed absorption peaks are caused by f–d electron transitions.⁵¹ The absorption spectrum of CePO_4

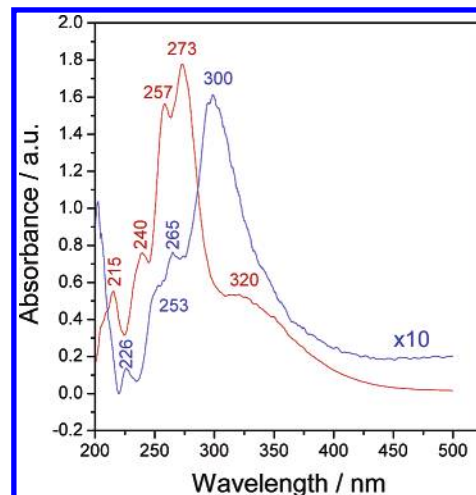


Figure 7. Absorption spectra of CePO_4 nanowires (red line) and bulk CePO_4 (blue line).

nanowires consists of five peaks with maxima at 215, 240, 257, 273, and 320 nm (Figure 7, red line), which correspond to the transitions from the ground state ${}^2F_{5/2}(4f^1)$ of Ce^{3+} to the five crystal field split levels of the $\text{Ce}^{3+} {}^2D(5d^1)$ excited states. It can be seen that the intensity of the peak at 273 nm is the strongest one. On the contrary, the absorption spectrum of bulk CePO_4 has four peaks with maxima appearing at 226, 253, 265, and 300 nm (Figure 7, blue line), in agreement with the reported values in the literature.^{50a} The peak at 300 nm shows the strongest intensity, which is different from that of CePO_4 nanowires. Moreover, the broad peak at 320 nm for CePO_4 nanowires was not observed for bulk CePO_4 , which may be attributable to the formation of low dimensional wirelike CePO_4 . This differential spectral behavior observed for CePO_4 nanowires and bulk CePO_4 might be ascribed to the distorted lattices. It is generally considered that the degree of disorder in the nano-materials is relatively high, thereby a lower crystal field symmetry might be induced in such materials.⁵² The cell volume of CePO_4 nanowires calculated from the XRD pattern is 280.41 \AA^3 , while the cell volume of bulk CePO_4 is 267.32 \AA^3 . The increase in the cell volume of CePO_4 nanowires indicates that the lattices are more distorted in the nanowires than in the bulk and that the crystal field symmetry is lower in the former than in the latter.⁵² Lower crystal field symmetry means that it is easy for the excited $\text{Ce}^{3+} 5d$ degenerate states to be completely split into five energy levels, and thus five peaks in optical absorption spectra of CePO_4 nanowires can be observed (Figure 7, red line). The lattice deformation may contribute to the change of band structure in nanowires, thus giving rise to the absorption peak shifts as compared with bulk material.

IV. Rare Earth Doped Hexagonal LnPO_4 Nanowires Synthesis and Photoluminescence. Eu^{3+} doped LaPO_4 nanowires were prepared by the hydrothermal method, and in this work, the concentration of dopant Eu ions is 5 mol %, so this phosphor can be expressed as $\text{La}_{0.95}\text{Eu}_{0.05}\text{PO}_4$. Figure S12 (Supporting Information) shows a representative TEM image of the obtained $\text{La}_{0.95}\text{Eu}_{0.05}\text{PO}_4$ product, and from the figure it

(49) (a) Milligan, W. O.; Mullica, D. F.; Beall, G. W.; Boatner, L. A. *Inorg. Chim. Acta* **1982**, *60*, 39. (b) Milligan, W. O.; Mullica, D. F.; Beall, G. W.; Boatner, L. A. *Acta Crystallogr.* **1983**, C39, 23.
 (50) (a) Imanaka, N.; Masui, T.; Itaya, M. *Chem. Lett.* **2003**, *32*, 400. (b) Imanaka, N.; Masui, T.; Hirai, H.; Adachi, G. Y. *Chem. Mater.* **2003**, *2003*, *15*, 2289.
 (51) Nakazawa, E.; Shiga, F. *Jpn. J. Appl. Phys.* **2003**, *42*, 1642.

(52) (a) Wei, Z.; Sun, L.; Liao, C.; Yin, J.; Jiang, X.; Yan, C. *J. Phys. Chem. B* **2002**, *106*, 10610. (b) Tao, Y.; Zhao, G.; Zhang, W.; Xia, S. *Mater. Res. Bull.* **1997**, *32*, 501. (c) Tissue, B. M. *Chem. Mater.* **1998**, *10*, 2837. (d) Williams, D. K.; Bihari, B.; Tissue, B. M.; McHale, J. M. *J. Phys. Chem. B* **1998**, *102*, 916.

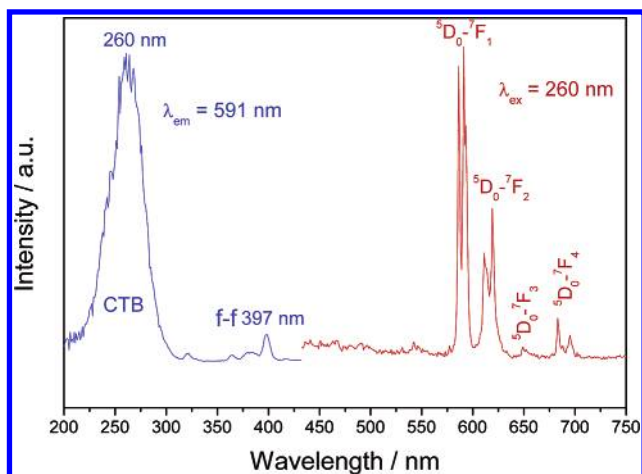


Figure 8. Excitation (blue line) and emission (red line) spectra of as-prepared $\text{La}_{0.95}\text{Eu}_{0.05}\text{PO}_4$ nanowires.

can be seen that the sample consists almost entirely of nanowires/nanorods with diameters of 5–30 nm and lengths of several micrometers.

The excitation spectrum obtained by monitoring the emission of LaPO_4/Eu nanowires is shown in Figure 8 (blue line). The broad band with a maximum at 260 nm shown in the spectrum originates from the excitation of the oxygen-to-europium charge-transfer band (CTB). By comparison with that of bulk LaPO_4/Eu (253 nm),⁵³ a small shift of the CT band could be observed for LaPO_4/Eu nanowires (260 nm). As reported by previous studies,^{52a,54} the peak position of the CT band is involved in the length of Eu–O bond; the longer the Eu–O bond is, the longer the wavelength of the CT band position will be. In this study, we have already pointed out that a relatively larger cell volume can be observed for LaPO_4/Eu nanowires compared to bulk LaPO_4/Eu . This indicates that the average Eu–O bond distance is relatively longer in LaPO_4/Eu nanowires, and as a consequence, a small redshift of the CT band would be observed. The general f–f transitions within the $\text{Eu}^{3+} 4f^6$ electron configuration in the longer wavelength region (300–500 nm) can also be observed (Figure 8, blue line). These peaks correspond to the direct excitation of the Eu^{3+} ground state into higher levels of the 4f-manifold such as ${}^7\text{F}_0\text{--}{}^5\text{L}_6$ at 397 nm. Upon excitation into the CTB of Eu^{3+} at 260 nm, the emission spectrum of powders of hydrothermally prepared LaPO_4/Eu nanowires (Figure 8, red line) consists of sharp lines as expected for the transitions between europium levels, which couple only very weakly to lattice phonons. Among ${}^5\text{D}_0\text{--}{}^7\text{F}_J$ ($J = 1, 2, 3, 4$) emission lines of Eu^{3+} shown in Figure 8 (red line), the magnetic-dipole transition ${}^5\text{D}_0\text{--}{}^7\text{F}_1$ (591 nm) is the most prominent group, which is characterized by orange-red emission. Emission from the higher energy levels (${}^5\text{D}_1$, ${}^5\text{D}_2$) of Eu^{3+} is not detected due to multiphoton relaxation based on the vibration of phosphate groups (ca. 1067 cm^{-1}), which can bridge the gaps between the higher energy levels (${}^5\text{D}_1$, ${}^5\text{D}_2$) and the lowest ${}^5\text{D}_0$ level of Eu^{3+} effectively. The intensity of transitions between different J -number levels depends on the symmetry of the local environment of the europium ions and can be described in terms

of the Judd–Ofelt theory.⁵⁵ The splitting observed in each group of luminescence lines (Figure 8, red line) is caused by the crystal field. The above luminescent properties of Eu^{3+} in the crystalline LaPO_4 nanowires are basically in agreement with those for bulk LaPO_4/Eu reported previously, indicating that Eu^{3+} ions have been successfully doped into host LaPO_4 nanowires. The transition (${}^5\text{D}_0\text{--}{}^7\text{F}_1$) displays more intensity than that of the transition (${}^5\text{D}_0\text{--}{}^7\text{F}_2$) due to localized energy transfer.

Although the transition energies are the same for nanowires and bulk particles, the intensity patterns of their luminescence spectra show small differences. Comparing bulk LaPO_4/Eu ^{52a} and LaPO_4/Eu nanowires, we find that the intensities of the lines belonging to the ${}^5\text{D}_0\text{--}{}^7\text{F}_4$ are different in the two cases. A similar difference can be observed for the components of the ${}^5\text{D}_0\text{--}{}^7\text{F}_2$ transition. The intensity of the luminescence lines of LaPO_4/Eu and other lanthanide doped phosphates is known to depend on the orientation of the unique crystal axis relative to the polarization vector of the incident light.⁵⁶ Since our excitation light was partly polarized, any preferred orientation of the nanowires in the powders will influence the intensity pattern of the emission spectra. Meanwhile, the ratio of the intensity of ${}^5\text{D}_0\text{--}{}^7\text{F}_1$ to ${}^5\text{D}_0\text{--}{}^7\text{F}_2$ for LaPO_4/Eu nanowires is smaller than that of bulk LaPO_4/Eu . Considering that the ${}^5\text{D}_0\text{--}{}^7\text{F}_2$ transition is hypersensitive to the symmetry of the crystal field, and it will be relatively strong if the symmetry of the crystal field is relatively low. By comparison with bulk LaPO_4/Eu , the increase of the intensity of the ${}^5\text{D}_0\text{--}{}^7\text{F}_2$ transition for nanowires is obviously correlated with the distorted lattices. The above results have demonstrated that the lattices are more distorted in the LaPO_4/Eu nanowires than in the corresponding bulk material.

In contrast to semiconductors such as CdSe, CdTe, and ZnO nanocrystals showing unique absorption and fluorescence characteristics due to quantum size effects,⁵⁷ the fluorescence of the LaPO_4/Eu nanowires originates from their bulk properties (i.e., transitions between d and f electron states and their local symmetry). In fact, particle size effects on the luminescence of LaPO_4/Eu nanowires are expected to be weak, since transitions of the well-shielded f electrons are mainly affected by the local symmetry of the crystal site.

V. Crystal Structure of LnPO_4 and the Possible Growth Mechanism of Hexagonal LnPO_4 Nanowires. In general, three kinds of mechanisms including vapor–liquid–solid (VLS) growth,⁵⁸ solution–liquid–solid (SLS) growth,⁵⁹ and template-mediated processes⁶⁰ have been proposed for the formation of crystalline nanowires. Clearly, the formation of the nanowires in our synthetic system would not be dominated by the above-mentioned three processes. To date, the shape of metal nanoparticles or semiconductor nanocrystals has mainly been controlled by the presence of surfactants, polymers or strong

(53) Yu, M.; Lin, J.; Fu, J.; Zhang, H. J.; Han, Y. C. *J. Mater. Chem.* **2003**, *13*, 1413.

(54) (a) Hoefdraad, H. E. *J. Solid State Chem.* **1975**, *15*, 175. (b) Tao, Y.; Zhao, G.; Ju, X.; Shao, X.; Zhang, W.; Xia, S. *Mater. Lett.* **1996**, *28*, 17.

(55) (a) Judd, B. R. *Phys. Rev.* **1962**, *127*, 750. (b) Ofelt, G. S. *J. Chem. Phys.* **1962**, *37*, 511.

(56) Meysamy, H.; Riwotzki, K.; Kornowski, A.; Naused, S.; Haase, M. *Adv. Mater.* **1999**, *11*, 840.

(57) (a) Peng, X.; Manna, L.; Yang, W.; Wickham, J.; Scher, E.; Kadavanich, A.; Alivisatos, A. P. *Nature* **2000**, *404*, 59. (b) Peng, Z. A.; Peng, X. G. *J. Am. Chem. Soc.* **2001**, *123*, 183. (c) Tang, Z.; Kotov, N. A.; Giersig, M. *Science* **2002**, *297*, 237. (d) Guo, L.; Ji, Y.; Xu, H.; Simon, P.; Wu, Z. *J. Am. Chem. Soc.* **2002**, *124*, 14864.

(58) Morales, A. M.; Lieber, C. M. *Science* **1998**, *279*, 208.

(59) Trentler, T. J.; Hickman, K. M.; Goel, S. C.; Viano, A. M.; Gibbons, P. C.; Buhro, W. E. *Science* **1995**, *270*, 1791.

(60) Harada, M.; Adachi, M. *Adv. Mater.* **2000**, *12*, 839. (b) Li, Y.; Li, X.; Deng, Z.; Zhou, B.; Fan, S.; Wang, J.; Sun, X. *Angew. Chem., Int. Ed.* **2002**, *41*, 33.

chelating ligands. Peng et al. presented a three-stage shape evolution mechanism based on the spherical diffusion controlled crystal growth theory, which elucidated the shape evolution of CdSe nanocrystals well.⁶¹ However, this theory has seldom been used to explain the formation mechanism of 1D nanowires/nanorods in surfactant-free systems. Yu et al. have recently reported the general synthesis of metal tungstate nanorods by the hydrothermal process and found that the formation process of the nanorods could fit the spherical diffusion model well.⁶² In our system, the formation of the nanowires could also be explained by this theory. Here, the strong pH-dependent relation with the lengths and aspect ratios of the nanowires is due to the sensitive influence of the pH on the solute concentrations ($[\text{Ln}^{3+}]$ and $[\text{PO}_4^{3-}]$). This observation suggests that the 1D growth stage was rightly captured by maintaining the solute concentrations in the correct range, through control of the pH. The obvious 1D growth stage observed here is also in agreement with the previous model proposed by Peng et al.⁶¹

LnPO_4 ($\text{Ln} = \text{La} \rightarrow \text{Dy}$) nanowires that were fabricated have a hexagonal crystal structure, similar to that of ZnO ⁶³ and $\text{Ln}(\text{OH})_3$,²⁵ which are well-known to exhibit anisotropic growth. Studying on the natural chemical character of lanthanide phosphates can help us to understand the growth mechanism of lanthanide phosphate nanowires. In this solution phase process, the morphology of the final product is largely determined by the anisotropic nature of the building blocks, that is, the 1D characteristics of the infinite linear chains of hexagonal structured LnPO_4 ($\text{Ln} = \text{La} \rightarrow \text{Dy}$) in the crystalline phase. The crystal structure of representative hexagonal CePO_4 is shown in Figure 9.⁶⁴ Each cerous ion is coordinated to eight oxygen atoms, four at distances of 2.34 Å and four at 2.66 Å. The shorter distances are to the corners of four different tetrahedra, linking atoms which are practically coplanar. The longer distances extend to pairs of oxygens forming the edges of two tetrahedra, one above and one below the plane of the four shorter distances. A given phosphate group is coordinated to six cerous ions, each corner by one short bonding distance, and opposite edges by longer bonding distances. The cerium–cerium separation is 4.13 Å. The phosphate ion has been taken to be a tetrahedral grouping of oxygens about phosphorus, with the P–O distance fixed at 1.56 Å (Figure 9a). The overall structure of this compound may be described as columns built up of alternate cerous and phosphate ions, extending along the c axis, each column linked to four neighboring columns is such that open channels run through the structure along the hexagonal axis (Figure 9b). The packing structure of hexagonal CePO_4 viewing along the a axis can be described as infinite linear chains, parallel to the c axis (Figure 9b). From a structural point of view, hexagonal CePO_4 consists of infinite linear chains extending along the c axis. From a thermodynamic perspective, the activation energy for the c axis direction of growth of hexagonal LnPO_4 is lower than that of growth perpendicular to the c axis.⁶⁵ This means a higher growth rate along the c axis and a lower one perpendicular to the c axis to form LnPO_4

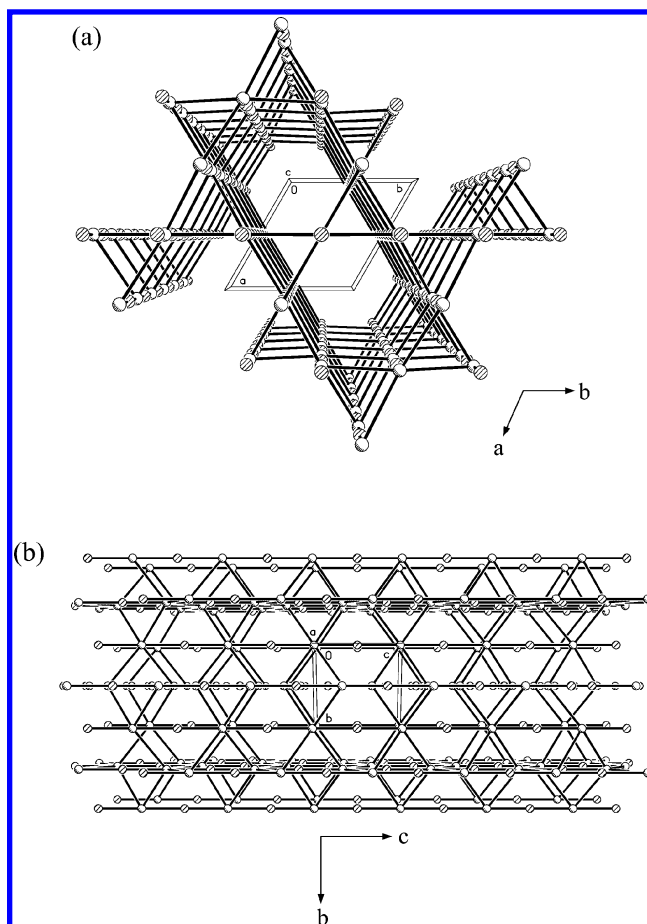


Figure 9. (a) Packing view of CePO_4 along the c axis. Each column is linked to four neighboring columns; open channels run through the structure along the hexagonal axis (the c axis). Oxygen atoms are omitted for clarity. (b) Packing view of CePO_4 along the a axis. Each column is built up of alternate cerous (shadow circles) and phosphate ions (open circles) and extends along the c axis. Oxygen atoms are omitted for clarity.

nanowires/nanorods that grow preferentially along the $[001]$ direction. This is in very good agreement with the abnormally strong intensity of the (200) peak in the XRD patterns (Figure S1, Supporting Information) and HRTEM results (Figures 5, S4, and S5). Hexagonal LnPO_4 ($\text{Ln} = \text{La}, \text{Pr}, \text{Nd}, \text{Sm}, \text{Eu}, \text{Gd}, \text{Tb},$ and Dy) are isostructural with hexagonal CePO_4 ; therefore, the formation of other LnPO_4 nanowires/nanorods can also be explained based on its highly anisotropic character along the c axis, in agreement with HRTEM observation (Figures 5, S4, and S5). It is this structural feature that plays a key role in the highly intrinsic preferential growth along the c axis of LnPO_4 ($\text{Ln} = \text{La} \rightarrow \text{Dy}$) nanowires.

On the contrary, tetragonal $(\text{Ho} \rightarrow \text{Lu}, \text{Y})\text{PO}_4$ has no preferred growth direction in the crystalline phase based on their crystal structure.⁴⁹ The molecular arrangements of tetragonal LuPO_4 viewing along the a , b , and c axis are presented in Figure 10a, b , and c , respectively. Compound LuPO_4 crystallizes in the tetragonal system conforming to space group $I4_1/amd$. The Lu atom is eight-coordinated to oxygen atoms with two unique metal–oxygen bond distances. Each of these discrete lengths are tetrahedrally oriented orthogonal to one another thus forming a distorted dodecahedron, which is a bisphenoid contains two interpenetrating distorted tetrahedra distinguished by the bond lengths $\text{Lu}-\text{O}'_s = 2.262 \text{ \AA}$ and $\text{Lu}-\text{O}'_s = 2.344 \text{ \AA}$. In other words, the eight vertexes of the dodecahedron are not equivalent

(61) (a) Peng, Z. A.; Peng, X. G. *J. Am. Chem. Soc.* **2001**, *123*, 1389. (b) Peng, Z. A.; Peng, X. G. *J. Am. Chem. Soc.* **2002**, *124*, 3343.

(62) Yu, S. H.; Liu, B.; Mo, M. S.; Huang, J. H.; Liu, X. M.; Qian, Y. T. *Adv. Funct. Mater.* **2003**, *13*, 639.

(63) Huang, M.; Mao, S.; Feick, H.; Yan, H.; Wu, Y.; Kind, H.; Weber, E.; Russo, R.; Yang, P. *Science* **2001**, *292*, 1897.

(64) Mooney, R. C. L. *Acta Crystallogr.* **1950**, *3*, 337.

(65) Murphy, K. E.; Altman, M. B.; Wunderlich, B. *J. Appl. Phys.* **1977**, *48*, 4122.

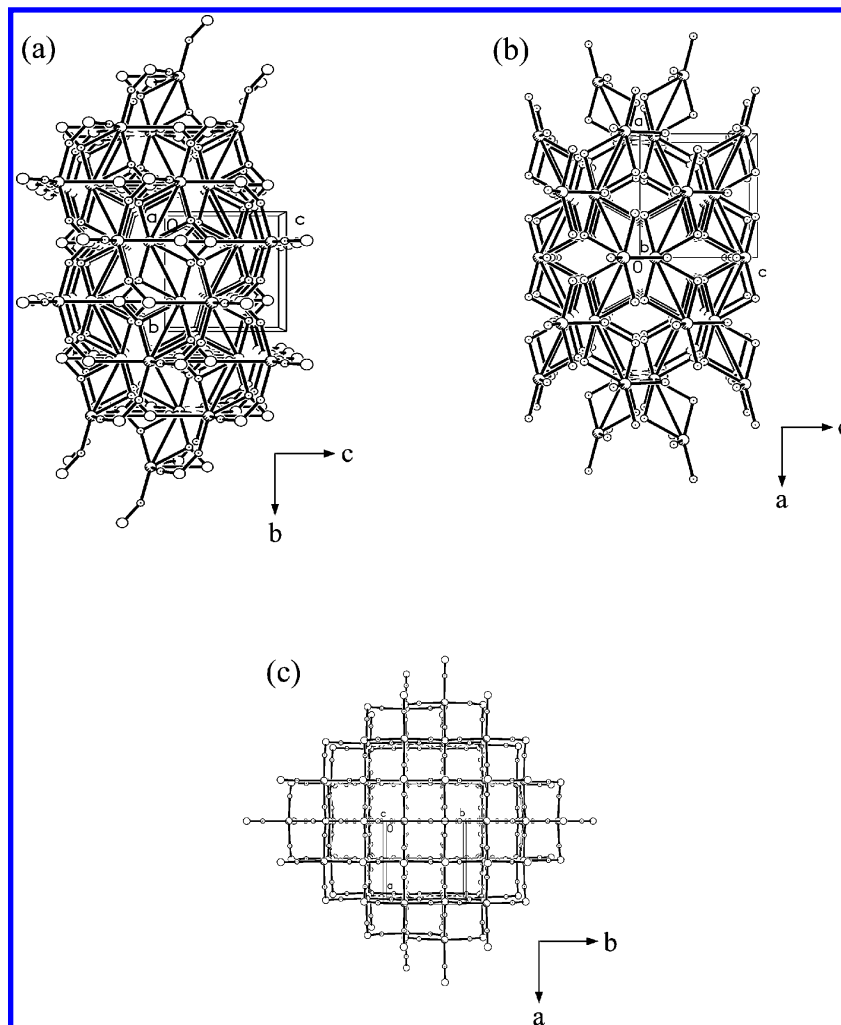


Figure 10. (a) Perspective view along the *a* axis of the molecular packing of LuPO_4 . (b) Perspective view along the *b* axis of the molecular packing of LuPO_4 . (c) Perspective view along the *c* axis of the molecular packing of LuPO_4 .

but are divided into two bisphenoidal sets, and those within each set are equal. The phosphate group PO_4 is a distorted tetrahedron with variable bond angles. No anisotropic nature can be observed in the tetragonal structured LuPO_4 , which is different from hexagonal structured CePO_4 . Therefore, the prepared LuPO_4 sample presents particle morphology instead of nanowires. Tetragonal HoPO_4 , ErPO_4 , TmPO_4 , YbPO_4 , and YPO_4 are isostructural with tetragonal LuPO_4 ;⁴⁹ therefore, the resulting irregularly shaped particle morphology can also be explained based on their crystal structure.

Conclusions

This article describes the development of a simple hydrothermal process for the systematic preparation of LnPO_4 crystals that have been preformed by a facile hydrothermal process. It has been found that lanthanide phosphates LnPO_4 crystallize with hexagonal or tetragonal structure depending on the ionic radius of the lanthanide ions. LnPO_4 ($\text{Ln} = \text{La} \rightarrow \text{Dy}$) nanowires/nanorods crystallize in the hexagonal form, while ($\text{Ho} \rightarrow \text{Lu}$, Y) LnPO_4 materials exist in the hexagonal structure under low-temperature hydrothermal conditions. The obtained hexagonal LnPO_4 ($\text{Ln} = \text{La}$, Ce , Pr , Nd , Sm , Eu , Gd , Tb , and Dy) products have wirelike morphology. On the contrary, tetragonal LnPO_4 ($\text{Ln} = \text{Ho}$, Er , Tm , Yb , Lu , Y) samples prepared under the same experimental conditions consist of irregularly shaped

particles. The structure transition of LnPO_4 ($\text{Ln} = \text{La} \rightarrow \text{Tb}$) nanowires/nanorods from the hexagonal to the monoclinic monazite can be observed, while their morphology is retained after calcination at 900°C in air. In the case of hexagonal DyPO_4 nanowires, they are transformed to tetragonal DyPO_4 nanowires by calcination. No phase change can be observed for the tetragonal structured ($\text{Ho} \rightarrow \text{Lu}$, Y) LnPO_4 after calcination. The as-synthesized LnPO_4 ($\text{Ln} = \text{La} \rightarrow \text{Dy}$) products consist almost entirely of nanowires/nanorods with diameters of 5–120 nm and lengths ranging from several hundreds of nanometers to several micrometers. Europium doped LaPO_4 nanowires were also successfully prepared. The absorption spectra of CePO_4 nanowires and photoluminescent properties of LaPO_4/Eu nanowires were reported. Based on the crystal structure of LnPO_4 , we suggest that the growth of LnPO_4 ($\text{Ln} = \text{La} \rightarrow \text{Dy}$) nanowires is determined by its highly anisotropic character along the *c* axis. The simplicity of the hydrothermal process, cheapness, and availability of raw materials, without the need for catalysts or templates, are important considerations for industrial manufacturing. Lanthanide phosphate nanowires could be doped with different lanthanide elements and used for fluorescent lamps, new type plasma display panels excited by ultraviolet radiation, and luminescent labels for biomolecules. We believe that other LnPO_4 phosphors with a wirelike morphology such

as LaPO_4/Tb , $\text{LaPO}_4/\text{Ce}/\text{Tb}$, and $(\text{La}, \text{Gd})\text{PO}_4/\text{Tb}$ can be prepared by the same method. Metal phosphates, also known as a component of bones and teeth, have proven to be inert and safe, with no known side effects to the human body. The features of lanthanide doped lanthanide phosphates are their high quantum yield, their high chemical stability, and their expected low toxicity, making them particularly suitable for biological labeling applications based on the individual rare earth doped LnPO_4 nanowire.

Acknowledgment. This work was supported by the National Natural Science Fund of China and the Guangdong Province “The Tenth Five-Year Plan” Key Projects (2001A1070103).

Supporting Information Available: XRD patterns; TEM and SEM images; EDS spectrum; FTIR spectra; XPS spectra (PDF). This material is available free of charge via the Internet at <http://pubs.acs.org>.

JA037280D